Micro air bubble manipulation by electrowetting on dielectric (EWOD): transporting, splitting, merging and eliminating of bubbles†

Yuejun Zhao and Sung Kwon Cho*

Received 2nd August 2006, Accepted 17th November 2006
First published as an Advance Article on the web 4th December 2006
DOI: 10.1039/b616845k

This paper describes various manipulations of micro air bubbles using electrowetting on dielectric (EWOD): transporting, splitting, merging and eliminating. First, in order to understand the response of bubbles to EWOD, the contact angle modulation is measured in a capped air bubble and confirmed to be in good agreement with the Lippmann–Young equation until saturation. Based on the contact angle measurement, testing devices for the bubble manipulations are designed and fabricated. Sequential activations of patterned electrodes generate continuous bubble transportations. Bubble splitting is successfully realized by activating a single electrode positioned in the middle of bubble base. However, it is found that there are criteria that make splitting possible only in certain conditions. For successful splitting, smaller channel gap, larger bubble size, wider splitting electrode and/or larger contact angle changes by EWOD are preferred. These criteria are verified by a series of experiments as well as a static analysis. Bubble merging is achieved by moving bubbles towards each other in two different channel configurations: (1) channel I, where bubbles are in contact with the bottom channel plate only, and (2) channel II, where bubbles in contact with the top as well as bottom channel plates. Furthermore, eliminating a bubble to the ambient air is accomplished. All the bubble manipulation techniques may provide a versatile integrated platform not only to manipulate micro objects by utilizing micro bubbles as micro carriers, but also to enable a discrete bubble-based gas analysis system.

1 Introduction

Bubbles are ubiquitous in everyday life. They have been one of the steady research topics for a long time, occupying an important place in physics, chemistry, engineering, medicine, and so on.[1,2] As such, their applications are diverse. Some examples include: boiling processes in energy generation, bubble injection in oil transport and production, gas–liquid reactors, floatation and separation of oils, minerals or biological cells, ink jet printers, and so on. In particular, in the past decades since the advent of microfluidic technology, micro bubbles have been attracting much more attention, not only bringing a great deal of interesting scientific/engineering issues, but also providing much potential in many microfluidic applications.

At the early stage of the microfluidics era, bubbles were largely regarded as necessarily avoided in microfluidic devices since they often cause clogging problems in narrow microfluidic passages.[3–5] However, as many control mechanisms over bubbles were developed, interests have transitioned to harnessing micro bubbles for actuating and regulating the surrounding fluids, as opposed to avoiding them.[6] Although various methods for bubble control have been introduced to date, they may be largely classified into three groups: thermal, electrochemical, and acoustic.

Among many thermal actuations, the most successful and thus most familiar application of bubbles would be thermal ink jet printers.[7] Rapidly growing bubbles by local heating can expel tiny ink droplets out of the nozzle in a controlled manner.[8,9] Also there have been reported many attempts to utilize thermally grown micro bubbles. Lin and his group[10–12] demonstrated that periodically growing and collapsing bubbles can push and pull a cantilever beam, and furthermore they can generate liquid pumping when actuated in the confined chamber with a nozzle and diffuser connected. Moving bubbles through the micro channel can also push the fluid filled in the channel.[13] Interestingly, thermally grown bubbles can be used for manipulating micro/bio particles. Maxwell *et al.*[14] used thermal bubbles positioned in a chamber to capture and release bio particles. In this configuration, there is no direct contact between the bubble and the bio particles since they are connected through a fluid conduit. However, the direct contact between bubbles and micro objects (for example, biological cells) is another option that provides more precise and flexible manipulations of micro objects. Since this contact involves soft bubbles, not any rigid materials, mechanical damage can be minimized. Taylor and Hnatovsky[15] and their continued work[16] demonstrated that bubbles thermally grown on an optical fiber tip can trap and mix particles as well as biological cells. However, this method is prone to thermal damage to biological objects. To obviate this problem, recently our group envisioned an electrowetting-actuated bubble

Department of Mechanical Engineering and Materials Science University of Pittsburgh, 3700 O'Hara St., Pittsburgh, PA, 15261, USA. E-mail: yuz21+@pitt.edu; Fax: +1-412-624-4846; Tel: +1-412-624-1769 E-mail: skc@engr.pitt.edu; Tel: +1-412-624-9798

† Electronic supplementary information (ESI) available: Schematic figures for capped bubble actuation, side view of testing device, bubble splitting criterion graph, electrode width effect on bubble splitting, and sequential images for bubble merging and eliminating out of bulk water. See DOI: 10.1039/b616845k

method by which micro objects can be trapped, pushed and pulled without any thermal damage.[17] More detailed results will be discussed in a different article.

The second approach to generate and collapse micro bubbles is to use the electrochemical method, so called electrolysis. Jackel *et al.*[18] may have been the first one to use electrochemically generated bubbles for bistable optical switching. Likewise, electrochemically generated bubbles can act as valves, pumps or other fluidic regulators.[19–23] The major advantage of this method over the thermal method is that the bubble temperature is close to room temperature. However, bubbles can only be generated primarily in electrolytes.

Another intriguing actuation method is so called acoustic streaming. Unlike liquid droplets, gaseous bubbles immersed in liquid are highly compressible in the presence of an acoustic field so that they oscillate (shrink and expand) in harmonic with the frequency of the acoustic field.[24] In particular, if the frequency coincides with the resonance frequency of the bubble, large oscillation amplitudes can easily be achieved, and thereby generate strong flow motions in the surrounding fluid. Marmottant and Hilgenfeldt[25] showed that high shear flows induced by an oscillating bubble can enhance the permeability of the neighbouring vesicles. In this case, the bubble can be used as a vector to deliver molecules or drugs into vesicles or biological cells. Recently, this acoustic streaming has been extended to steering micro fluid flows[26] by carefully combining bubbles with solid structures, in the hope of developing a new microfluidic device that does not require any conventional micro channel networks.

Besides the above works, other bubble actuations have been developed, such as bubble creation by hydrodynamic focusing[27–29] or T-junctions,[30–32] bubble venting using a degassing plate[33] and so on. However, most of the bubble actuations listed above remain inflexible and limited in degree of freedom, allowing only simple bubble operations such as growing and collapsing in a fixed spot or moving only along a confined path (micro channel). There have been very few studies on single or multiple bubble manipulation with high degree of freedom in a two- or three-dimensionally open space. Recently, Ito *et al.*[34] showed electrostatic actuations by which bubbles can be transported and merged along arrayed electrodes on a two dimensional plate, demonstrating a chemical reaction between two gas reagents. The bubble environment was filled with oil. However, their operations are limited to only two types: transporting and merging of bubbles in an oil environment. Furthermore, their electrostatic actuations require high voltage (up to several hundreds volts).

In the present paper, we use the electrowetting principle (to be exact, electrowetting on dielectric or EWOD) to drive gaseous bubbles in an aqueous environment. This configuration offers two main advantages. First, the use of EWOD facilitates various reliable operations (transporting, splitting, merging, and eliminating) of single or multiple bubbles with high degree of freedom and precision. Second, the bubble operations in an aqueous environment may allow bubbles to be used as micro carriers that manipulate micro objects (cells) in a bio solution through direct yet soft contacts with the objects.

The present work begins with a fundamental study on EWOD actuations in a capped air bubble. The contact angle modulation under EWOD is measured. Then, these data are used not only for device design and fabrication but also for static analysis in the bubble splitting process. Afterwards, based on the contact angle measurement and analysis, four bubble operations (transporting, splitting, merging and eliminating) are realized. Some preliminary results[35] have previously been reported in a conference. In this paper, particular emphasis is placed on the bubble splitting process. All these bubble operation units may be used to manipulate micro objects by utilizing micro bubbles as micro carriers.[17] As another possible application, they may also be used for a discrete bubble-based gas analysis system.

2 Electrowetting on dielectric (EWOD) in capped bubbles

2.1 Background

Lippmann[36] first recognized over 100 years ago that an externally added electrostatic charge may significantly modify the capillary forces at an interface. However, this phenomenon had not drawn much attention until the MEMS technology emerged. Recently, however, many reports have shown that the phenomenon also prevails in configurations where the electrode is covered with a thin dielectric layer[37] (see Mugele and Baret[38] for an extensive review). The wettability of liquids on a dielectric surface can be electrically controlled with high reversibility in many cases.

For example, consider an aqueous droplet beneath which hydrophobic dielectric layers and an electrode are placed in series entirely covering the droplet base area (refer to Fig. S1(a) in the ESI†). When the electric voltage V is applied between the aqueous sessile droplet and the electrode, the droplet spontaneously spreads out on the dielectric surface. The contact angle θ is modulated by the applied voltage according to the Lippmann–Young equation:

$$\cos\theta = \cos\theta_o + \frac{\varepsilon\varepsilon_0}{2\gamma_{lg}t}V^2 \quad (1)$$

where ε_0 denotes the permittivity of the vacuum, ε the dielectric constant of the dielectric layer, γ_{lg} the gas-to-liquid interfacial tension and t the thickness of the dielectric layer. This contact angle modulation can also be described using electrohydrodynamic approaches.[39,40] When the electric potential V is removed, the changed contact angle returns to the initial contact angle θ_o. This method, called electrowetting on dielectric (EWOD), is an excellent tool to access and control the fluid interfaces. Different methods such as electrochemical,[41] dielectrophoretic,[42,43] thermal,[13,44,45] and optical[46] can also be used to access and control the fluid interfaces. However, EWOD provides the following outstanding features: (1) excellent reversibility; (2) extremely low power consumption (less than μW) since the dielectric layer acts like a capacitor, not a energy dissipation part; and (3) superb robustness since there is no direct electrochemical interaction between the electrode and liquid.

To date, a great number of studies on EWOD from fundamentals[36,37,39,47] to droplet manipulations[48–51] and practical applications[52–55] have been done with aqueous liquid droplets in an air or oil environment. However, data for gaseous bubble actuations by EWOD are not currently available in many cases. It is anticipated that a gaseous bubble in an aqueous liquid can also be controlled by EWOD. Suppose a capped air bubble immersed in the aqueous liquid is placed on a hydrophobic dielectric surface (Fig. S1(b)). Note that the contact angle θ is also defined in the liquid side. When the voltage V is applied between the liquid and the electrode, the contact angle θ would be decreased according to eqn. (1). As a result, the gaseous bubble sitting on the dielectric surface would spontaneously contract from the original state. This process is reverse to the droplet case. Applying the electric voltage induces a contraction in the bubble instead of spreading. When the electric voltage is removed, the bubble spreads and returns to the initial state since the dielectric surface changes back to the initial hydrophobic state. This bubble actuation would also be highly reversible. In order to confirm this behaviour, the contact angle modulation in bubbles is first measured under EWOD actuation.

2.2 Measurement of contact angle in capped bubble

For contact angle measurements in an EWOD actuated bubble, a DI water reservoir was made of four glass faces on the side and a bottom plate, the surface of which was covered with a 2000 Å Au electrode layer, a 1 μm dielectric parylene layer and a 2000 Å Teflon layer in series. Here the layers covered the entire surface of the bottom plate (Fig. S1). After pouring DI water (resistivity ~ 18 MΩ cm) into the reservoir, an air bubble of about 1 μL in volume was injected on to the bottom plate using a pipette. Fresh air bubbles and DI water were used in every measurement to minimize any effects of trapped charges. The adjustable DC voltage was applied between the electrode underneath the dielectric layer and the probe which was inserted into the water solution. Most of the experiments were carried out with applying a positive signal on the probe and grounding on the substrate electrode. We could not observe any noticeable change in contact angle when the polarity was reversed. Each time the applied voltage changed, side views of the bubble were captured by a microscope (VZM™ 450i, Edmund Optics Inc.) and a CCD camera (JAI® CV-S3200). The corresponding contact angle was analyzed using a graphic tool (Microsoft® Office Visio® Professional 2003). This measurement procedure was repeated 3–5 times for each voltage, and the measured data were averaged.

Fig. 1 shows that the measured contact angle is in reasonably good agreement with eqn (1) up to an applied voltage of about 80 V_{DC}. Over 80 V_{DC}, the contact angle does not decrease much but starts to flatten out, which is well known as contact angle saturation. From these experimental data, the behaviour of contact angle in the bubble configuration, including the saturation phenomenon, is confirmed to be very similar to the one in the droplet configuration. This means that eqn (1) is also valid in describing EWOD actuations of bubbles as well as droplets. The main difference is only the resultant change in overall bubble shape, as shown in the insets in Fig. 1: contracting in the bubble *vs.* spreading in the droplet with EWOD on, and *vice versa* with EWOD off.

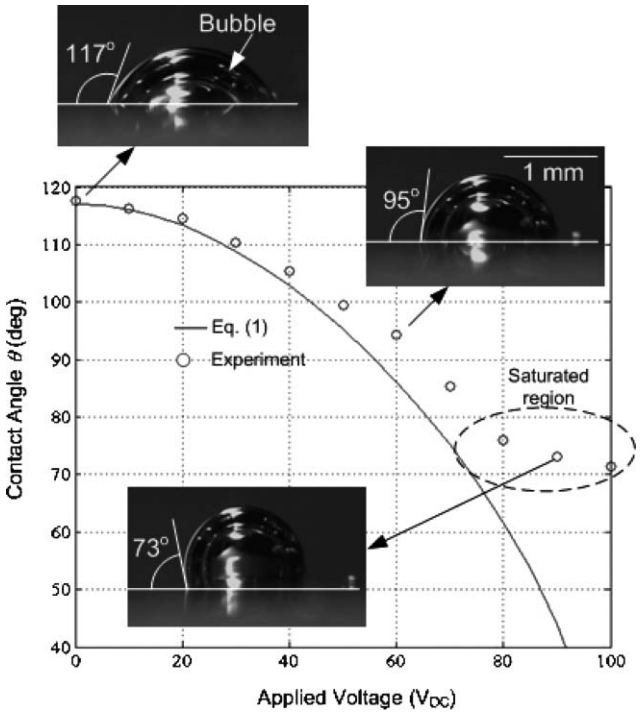

Fig. 1 Contact angle measurement in a capped bubble (volume ~ 1 μL) under EWOD. As the applied voltage increases, the contact angle decreases and as a result the bubble contracts. Over about 80 V_{DC}, the contact angle is saturated. The insets show the side view at the corresponding contact angle.

3 Bubble operations

3.1 Transporting of air bubble

Using the EWOD principle, air bubbles can be continuously transported by sequentially activating an array of individually addressable control electrodes. A schematic for the driving mechanism is illustrated in Fig. S2.† If any of the electrodes over which a bubble is partially placed is activated, the bubble can be transported. For example, the activation of the first electrode from the right in Fig. S2† makes the bubble move left. Since the contact angle on the activated area decreases according to eqn (1), the resultant of interfacial forces on the bubble is directed to the left. Another interpretation is that since the bubble is fond of staying on a hydrophobic surface, it moves (is repelled) away from the activated (hydrophilic) surface to the next hydrophobic surface. Consequently, this activation acts as generating a "pushing" force by which the bubble is moved away from the activated electrode area. In droplet driving, on the contrary, the activation has a pulling effect.

3.1.1 Fabrication of testing device. In order to test the bubble operating scheme, testing devices were fabricated using standard lithographic micro fabrication technology. The testing devices mainly consist of two parallel plates (top and bottom), as shown in Fig. S2.† The main fabrication process

on the bottom plate consists of three steps: metallization and patterning of control electrodes, deposition and patterning of the dielectric layer, and deposition of the hydrophobic layer. For the control electrodes, a chromium layer of 100 Å in thickness as an adhesion layer and a gold layer of 1000 Å in thickness were sequentially deposited on a glass wafer by sputtering and then patterned by wet etching. Typically the control electrode for bubble transporting, merging and eliminating is a square type with an area of 1.4 × 1.4 mm^2 while the splitting electrode is a long rectangle type with four different widths (1.4 mm, 600 μm, 200 μm and 100 μm). Then, a 1 μm parylene layer as the dielectric layer was deposited using a chemical vapour deposition process (Specialty Coating Systems, PDS-2010 LABCOTER® 2), followed by opening of the parylene layer on electrode pads by physical scratching in order to transmit activation signals to each control electrode. Finally, the bottom plate was finished with a hydrophobic Teflon layer. Spin-coating of 2% Teflon solution (Teflon AF 1600® + Fluorocarbon solvent) results in a 2000 Å thick Teflon layer.

The top glass cover, coated with an ITO (Indium Tin Oxide) layer, was also spin-coated with the hydrophobic Teflon layer. The transparent ITO layer covering the entire area of the top glass cover makes bubble motions observable. The last step of the fabrication process is to integrate the two plates. After putting a large water drop on the bottom plate and then injecting air bubbles, the top cover plate was gently pressed against the spacers that were already placed in the four corners on the bottom plate. Double-sided tape was used for the spacers. The gap between the top and bottom plates was adjusted by the number of tape layers of which thickness was measured using a profiler (Veeco Dektak® 3 ST Surface Profile Measurement System). Depending on the channel gap, the testing channel can be divided into two types: (1) channel I where the bubble is in contact with the bottom plate only; and (2) channel II where the channel gap is small enough for the bubble to be in contact with both top and bottom plates.

To generate activating signals, a personal computer, a digital output board (DAQPad-6507, National Instrument), and a custom-made interface circuit mainly containing photo-coupled relays (PhotoMos®, AQW614EH, Aromat Co.) were incorporated. A PC-based program generated control signals transmitted through the digital I/O board. The control signals switched the relays that provided activation voltages to the electrodes on the testing devices. The applied voltage to the electrodes was adjustable but mostly set at $V = 90\ V_{DC}$, where the contact angle was saturated. This configuration of testing device was used for all the bubble operations of merging, splitting, eliminating as well as transporting.

3.1.2 Testing results of transporting. Shown in Fig. 2 are the experimental results verifying the scheme of air bubble transporting in channel I where the bubble is in contact with the bottom plate only. Besides, similar transportations are also achieved (not shown) in channel II where the bubble is in contact with both top and bottom plates. As shown in Fig. 2(a), an air bubble is initially sitting over two electrodes, covering the right one more than the left one. None of the electrodes are activated yet. Immediately after the left electrode of the two is activated, the air bubble starts to move right very quickly. It takes the air bubble less than 0.03 sec to completely move to the next right electrode. Subsequently, the right electrode is also activated together with the left one. The air bubble moves again to the right. Finally, the air bubble is placed on the right edge of its initial sitting area, as shown in Fig. 2(b).

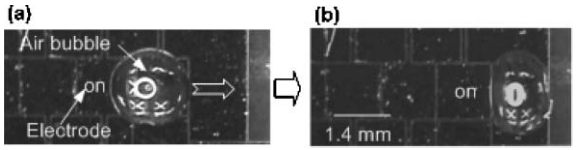

Fig. 2 Sequential photos of air bubble transporting: (a) before EWOD actuation; (b) the bubble moves one step right immediately after activating the electrode placed on bubble's left. After repeating activation again, the bubble is finally placed on the right edge. The images are viewed through the top transparent glass plate. Note that the bubble is in contact with the bottom plate only (channel I).

In essence, activating of electrodes generates a "pushing" force, thus repelling the bubbles away from the activated area. Unlike droplet transportation, where the activation essentially generates a "pulling" force, this sometimes causes bubbles to move sideways (not straight forward) depending on how they are initially positioned on the activated area. This occasionally results in running off the straight track. However, this problem was overcome by installing guide electrodes on both sides of the track and activating them together with the pushing electrode.

3.2 Splitting of air bubble

Fig. 3 schematically describes how a single bubble can be split. Only one bottom electrode (long rectangle) placed in the

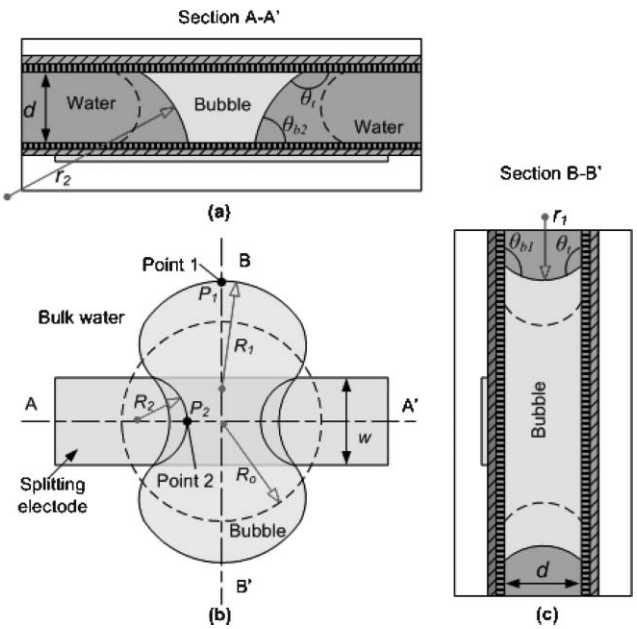

Fig. 3 Bubble configuration for splitting in channel II: (a) cross-sectional view along A-A′; (b) plan view; and (c) cross-sectional view along B-B′. Activating the splitting electrode placed in the middle of bubble base makes the bubble pinched and then split completely. Broken lines indicate the initial shape of the bubble and open arrows denote the radii of principal curvature of the interface at points 1 and 2.

middle of the bubble base is activated. Initially a bubble with radius R_o, shown by broken lines, is centred on the splitting electrode of width w. In this configuration, we limit our scope to the case where $R_o > w/2$. If the splitting electrode entirely covers the bubble base area, the bubble cannot be split by this method. Note that the bubble contacts the top plate as well during the splitting process (channel II). This condition is not necessarily required in bubble transporting, merging and eliminating. In order to perform splitting, the splitting electrode is first activated, and then the surface over the activated electrode becomes hydrophilic. During this process other areas remain hydrophobic. As a result, the middle part of the bubble is pinched (necking) and the bubble is overall elongated in the longitudinal direction to keep the total volume of the bubble constant. Once two pinched menisci meet together near the bubble center, the bubble will be completely split into two daughter bubbles. This splitting operation can be used to make the bubble size comparable to micro objects in the micro bubble carriers or to control the gas volume in the discrete bubble-based gas analysis system.

3.2.1 Static analysis of bubble splitting process. To understand the physics of bubble splitting, the splitting process is analysed. The static analysis for droplet splitting was detailed in Cho *et al.*[48] In the analysis, the key principle was that the pressure inside the droplet is uniform when in equilibrium. The similar principle can be applied to analyze the bubble splitting process. However, a distinctive feature is that the geometrical configuration is reversed. In addition, the effect of the electrode width w is also experimentally investigated.

When a bubble is squeezed between two plates, the radii of the meniscus in the bubble r (open arrows in Fig. 3(a) and (c)) are geometrically related to the local contact angles θ and the channel gap d, as:

$$r_1 = \frac{-d}{\cos\theta_t + \cos\theta_{b1}} \tag{2}$$

$$r_2 = \frac{-d}{\cos\theta_t + \cos\theta_{b2}} \tag{3}$$

where subscripts t and b indicate the top and bottom plates and subscripts 1 and 2 denotes points 1 and 2 in Fig. 3(b) (that is, the end and middle regions of the bubble on the bottom plate), respectively. These relations are derived based on the assumption that the meniscus shape in Fig. 3(a) and (c) is a circular arc because the gravity effect is negligible in the scale of current interest. The Laplace equation gives the pressure difference across the bubble interface as follows:

$$P_L - P_1 = \gamma_{lg}\left(\frac{1}{r_1} + \frac{1}{R_1}\right) \tag{4}$$

$$P_L - P_2 = \gamma_{lg}\left(\frac{1}{r_2} + \frac{1}{R_2}\right) \tag{5}$$

where R is the principal radius of curvature, which is defined positive when drawn in the liquid side as shown in Fig. 3(b) and P_L the pressure of liquid. In a static equilibrium, the pressure should be equal everywhere inside the bubble, that is, $P_1 = P_2$. After eliminating r_1 and r_2, eqn (2–5), the equilibrium conditions are reduced to:

$$\frac{R_2}{R_o} \cong \frac{1}{\frac{R_o}{d}(\cos\theta_{b2} - \cos\theta_{b1}) - 1} \tag{6}$$

Note that since the meniscus shape near point 1 in Fig. 3(b) does not change substantially from the initial shape, R_1 can roughly be assumed equal to the initial bubble radius R_o in magnitude but negative in sign. Eqn (6) provides an important criterion for bubble splitting. The splitting is initiated by pinching the middle of the bubble. In other words, R_2 has to change from initially negative ($-R_o$) to positive. Eqn (6) reveals that this condition is more likely to be reached when the contact angle change by EWOD is larger (*i.e.*, large positive value of $\cos\theta_{b2} - \cos\theta_{b1}$), the channel gap d is smaller and/or the bubble size R_o is larger.

Recall that θ_{b2} is modulated by EWOD according to eqn (1) while θ_{b1} is constant and equal to the initial contact angle θ_o, since there is no EWOD electrode activated at point 1. Using eqn (1), eqn (6) may be re-written with the EWOD voltage V that is applied across the bottom dielectric layer, as

$$\frac{R_2}{R_o} \cong \frac{1}{\frac{R_o}{d}\left(\frac{\varepsilon\varepsilon_0}{2\gamma_{lg}t}V^2\right) - 1} \tag{7}$$

It is optimal that the applied voltage is set at 90 V_{DC}, where the contact angle starts to saturate as shown in Fig. 1. This voltage will make the change in contact angle maximize. At higher voltages, the dielectric layer is prone to break down without any considerable change in contact angle. At 90 V_{DC}, it is assumed that $\theta_{b1} \approx 117^\circ$ and $\theta_{b2} \approx 73^\circ$, as shown in Fig. 1. Based on this contact angle change, the relation among d, R_o and R_2 is plotted using eqn (6), as shown in Fig. S3.†

If R_o/d is below 1.34, R_2 is negative, which means the bubble remains without necking. However, if R_o/d is above 1.34, R_2 will become positive, resulting in necking in the middle of the bubble. Consequently, in order to have a pinched neck, the bubble size has to be necessarily larger than 1.34d or the channel gap d smaller than R_o/1.34. However, this condition does not guarantee *complete* splitting. In order to complete the splitting, two necking-in menisci have to meet near the centre of the bubble. It turns out that this is highly dependent on the splitting electrode width w as discussed in the next section.

3.2.2 Testing results of splitting. Shown in Fig. 4 is a series of experiments performed to verify the criterion for successful bubble splitting. First, the channel gap effect is investigated as shown in Fig. 4(a)–(c). In this case, the splitting electrode width and the applied voltage V are fixed at 1.4 mm and 90 V_{DC}, respectively. The bubble size R_o is also fixed around 1.3 mm. When the channel gap d is set at 240 μm, as shown in Fig. 4(a), bubble splitting cannot be achieved at all. Even the bubble necking seldom occurs, although the bubble is elongated after it reaches a static equilibrium. When the applied voltage is raised to 210 V_{DC}, necking in the middle occasionally occurs. However, at this voltage or over 210 V_{DC}

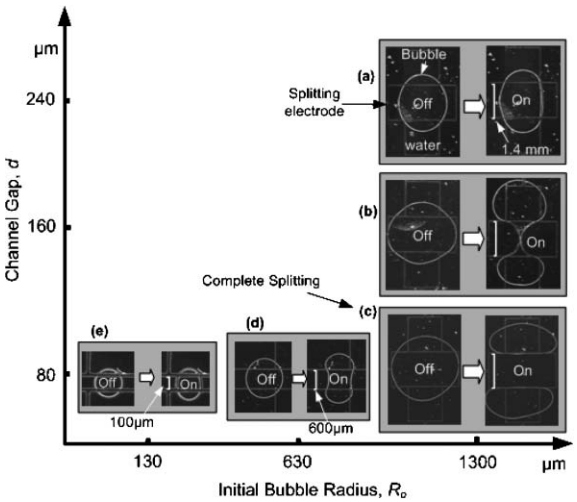

Fig. 4 Experimental verification of the bubble splitting criterion. In each case images are taken before (shown left) and after (shown right) activating the splitting electrode: (a)–(c) the effect of the channel gap d with a fixed R_o ($\approx$1300 μm). As d decreases, the bubble is further pinched in the middle and finally split into two (c); and (c)–(e) the effect of the bubble size in the condition that the ratio of the splitting electrode width and the bubble size w/R_o is about equal in all the three cases. The smaller the bubble, the more difficult it is to reach pinched shapes in the middle. Bubble volumes in (a)–(e) are 1.00, 0.87, 0.45, 0.10 and 0.004 μL, respectively. The same voltage of 90 V_{DC} is applied in all the five cases.

electrolysis and electric breakdown easily occur, as a result damaging the surface of the testing devices. The static analysis predicts that the necking is supposed to occur as long as d is smaller than about 0.97 mm ($\approx$1.3 mm/1.34). It is speculated that this discrepancy is due mainly to the contact angle hysteresis.[56–58] The contact angles assumed in the static analysis may be different from the actual contact angles when the bubble is squeezed and dynamically moving in the channel. The different contact angles give different critical values of d/R_o at which the phase of bubble necking is divided. For a more accurate prediction, the contact angle hysteresis should be taken into account in eqn (6).

Nevertheless, the static analysis predicts the trend very well as follows. When the channel gap is reduced to 160 μm, we can clearly see bubble necking in the middle of the bubble where two concave menisci are almost in contact (Fig. 4(b)). However, the splitting is not complete yet. It seems that the two menisci on the top plate are not in contact although on the bottom plate they may or may not be in contact since the EWOD actuation is applied only on the bottom plate. When the channel gap is reduced further down to 80 μm, the bubble is completely pinched off and then successfully split into two daughter bubbles, as shown in Fig. 4(c). This series of results suggests that, for a given condition, the channel gap has to be reduced enough to ensure complete splitting. This also explains why we could not split bubbles that were configured in channel I. To more accurately predict the channel gap required for successful splitting, the contact angle hysteresis should be measured.

The effect of the bubble size is also investigated as shown in Fig. 4(c)–(e). As the bubble becomes smaller for a given channel gap (80 μm), the extent of necking becomes less. This reveals that the smaller bubble size, the more difficult the splitting becomes. Note in Fig. 4(c)–(e) that the ratio between the splitting electrode width and the bubble radius w/R_o is maintained nearly equal in the three cases. From this series of experiments, it is clearly shown that the channel gap d and the bubble size R_o are critical factors to successfully split a bubble. Moreover, the trend that smaller channel gap and/or larger bubble size make bubble splitting easier is in good agreement with the static analysis.

Another interesting issue is the effect of the splitting electrode width w. Fig. S4† shows bubble splitting behaviours in three different electrode widths (100, 200 and 600 μm). In all the cases, the gap d and the applied voltage V are fixed at 80 μm and 90 V_{DC}, respectively. Also the bubble radius R_o is fixed around 900 μm. As shown in Fig. S4,† necking occurs in all three cases since the channel gap is small enough. However, only when w = 600 μm (Fig. S4(c)), is the splitting successfully completed. As w decreases, the two menisci do not move deeply into the centre of the bubble (Fig. S4(a) and (b)). This means that it is more likely to split the bubble when the electrode width is larger.

Sequentially captured pictures for the complete splitting process are shown in Fig. 5. Upon activating the splitting electrode, the menisci move into the centre of the bubble (Fig. 5(b)). Once the two menisci meet together, the splitting is finally completed, thereby producing two separate daughter bubbles (Fig. 5(c)). This whole splitting process is completed within a second in most cases.

3.3 Bubble merging

In bubble merging, two different channel configurations are considered: channel I and channel II. In channel II, bubble merging is achieved by moving two bubbles towards each other. This can be realized by activating each electrode over which the corresponding bubble is sitting on while the middle electrode is off, as shown in Fig. 5(c) and (d). This can be the reverse process to the splitting process. The applied voltage ranging between 50 and 90 V_{DC} is tested. Higher voltages can make merging faster. More interestingly, it is observed that larger and smaller water droplets are created inside the merged bubble after complete merging (Fig. 5(d)). In Fig. 5(d), the larger droplet is in contact with the top and bottom plates while the smaller droplets in contact with the top plate only. Their creation mechanisms seem to be different. The larger one

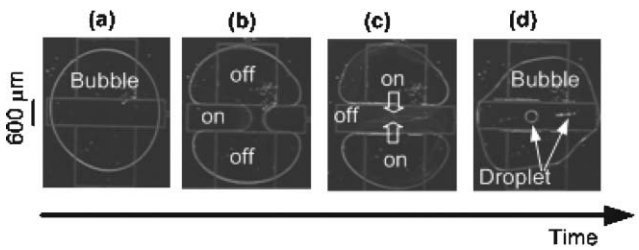

Fig. 5 ((a)–(c)) Sequential images of successful splitting and ((c) and (d)) merging of bubbles (d = 80 μm, w = 600 μm, bubble volume = 0.45 μL and applied voltage = 90 V_{DC}). Note that after merging, larger and smaller droplets are formed inside the merged bubble in (d).

is seemingly produced by laterally non-uniform advancing speed of the menisci. On the other hand, the smaller ones are due to the fact that the EWOD actuation is installed only on the bottom plate. The menisci on the bottom plate lead and thereby merge earlier than the ones on the top plate. In this case, a long liquid water column in parallel to the moving meniscus lines would be formed on the top plate. Since this column is hydro-dynamically unstable as far as it is in contact with one hydrophobic solid surface only (top plate),[48] it spontaneously breaks into small droplets. Similar water droplet formations are also observed at different applied voltages. Generally, as the applied voltage is lower, it is more likely to create smaller droplets than larger ones but with higher populations.

In channel I, bubble merging is similarly achieved by moving one bubble to another. Sequential images are shown in Fig. S5(a).† In this channel system, no droplet is created inside the merged bubble since there exists a semi-infinite open space above the bubbles such that all water between the two bubbles can easily escape to the bulk liquid space. The merging process can be used to mix different types of gases or to control the volume of discrete bubble.

3.4 Bubble eliminating

The experimental results of air bubble eliminating out of the bulk water solution are shown in Fig. S5(b).† By moving the air bubble on to the air-to-water interface of bulk water solution, the air bubble is quickly removed into the ambient air surrounding the bulk water solution.

4 Conclusions

In this paper, various air bubble manipulations (transporting, splitting, merging and eliminating) by the electrowetting on dielectric (EWOD) principle are described. First, in order to understand bubble behaviour under EWOD actuation, contact angle measurements are made in a capped air bubble. It is confirmed the contact angle is well modulated by EWOD following the Lippmann–Young equation until being saturated above the saturation voltage, as similarly occurs in the droplet configuration. However, the overall bubble response to EWOD actuation is reversed to the one in the droplet: contracting in the bubble *vs.* spreading in the droplet with EWOD on, and *vice versa* with EWOD off. It is demonstrated that bubbles can be continuously transported by sequentially activating patterned electrodes. In the bubble splitting process, one splitting electrode which is placed in the middle of the single bubble base is activated. It is found that the four main parameters (channel gap, bubble size, contact angle change, and splitting electrode width) come into critical play in successful splitting. In order to successfully complete the splitting process, smaller channel gap, larger bubble size, larger electrode width and/or larger contact angle change are preferred, which is in good agreement with the criteria derived from the static equilibrium condition and geometrical analysis.

Bubble merging is achieved by moving bubbles toward each other. During the merging process, more interestingly, isolated droplets inside the merged bubble are created when the bubbles are initially configured in contact with the top as well as bottom plates. However, there is no droplet generated after bubble merging when the bubbles are in contact with the bottom plate only. It is demonstrated that a bubble can be eliminated to the surrounding air by moving it to the air–water interface of the bulk water.

Although all the bubble operations described above are performed on separate chips, they can be monolithically integrated on a single chip in the future. Thereby, the bubble manipulation techniques may provide a versatile integrated platform not only to manipulate micro objects by utilizing micro bubbles as micro carriers but also to enable a discrete bubble-based gas analysis system.

Acknowledgements

The work was supported by the National Science Foundation (NSF ECS-0601470) and the SITE (Swanson Institute for Technical Excellence) Program.

References

1 D. Lohse, Bubble puzzles, *Phys. Today*, 2003, **56**, 36.
2 V. S. Ajaev and G. M. Homsy, Modeling shapes and dynamics of confined bubbles, *Annu. Rev. Fluid Mech.*, 2006, **38**, 277–307.
3 P. Gravesen, J. Branebjerg and O. S. Jensen, Microfluidics–a review, *J. Micromech. Microeng.*, 1993, **3**, 168–182.
4 M. J. Jensen, G. Goranovic and H. Bruus, The clogging pressure of bubbles in hydrophilic microchannel contractions, *J. Micromech. Microeng.*, 2004, **14**, 876–883.
5 M. Elwenspoek, T. S. J. Lammerink, R. Miyake and J. H. J. Fluitman, Towards integrated microliquid handling systems, *J. Micromech. Microeng.*, 1994, **4**, 227–245.
6 C.-J. Kim, 30th AIAA Fluid Dynamics Conference, Norfolk, VA, 1999, 1–6.
7 N. J. Nielsen, History of thinkjet printhead development, *Hewlett–Packard J.*, 1985, **36**, 4–10.
8 F.-G. Tseng, C.-J. Kim and C.-M. Ho, A high-resolution high-frequency monolithic top-shooting microinjector free of satellite drops – part i: Concept, design, and model, *J. Microelectromech. Syst.*, 2002, **11**, 427–436.
9 F.-G. Tseng, C.-J. Kim and C.-M. Ho, A high resolution high frequency monolithic top-shooting microinjector free of satellite drops: Part ii: Fabrication, implementation, and characterization, *J. Microelectromech. Syst.*, 2002, **11**, 437–447.
10 L. W. Lin, Microscale thermal bubble formation: Thermophysical phenomena and applications, *Microscale Thermophys. Eng.*, 1998, **2**, 71–85.
11 J. H. Tsai and L. W. Lin, A thermal-bubble-actuated micronozzle-diffuser pump, *J. Microelectromech. Syst.*, 2002, **11**, 665–671.
12 J. H. Tsai and L. W. Lin, Active microfluidic mixer and gas bubble filter driven by thermal bubble micropump, *Sens. Actuators, B*, 2002, **97-8**, 665–671.
13 T. K. Jun and C.-J. Kim, Valveless pumping using traversing vapor bubbles in microchannels, *J. Appl. Phys.*, 1998, **83**, 5658–5664.
14 R. B. Maxwell, A. L. Gerhardt, M. Toner, M. L. Gray and M. A. Schmidt, A microbubble-powered bioparticle actuator, *J. Microelectromech. Syst.*, 2003, **12**, 630–640.
15 R. S. Taylor and C. Hnatovsky, Trapping and mixing of particles in water using a microbubble attached to an nsom fiber probe, *Opt. Express*, 2004, **12**, 916–928.
16 M. Diop and R. Taylor, Soft trapping and manipulation of cells using a disposable nanolitre biochamber, *Biophys. J.*, 2006, **90**, 3813–3822.
17 Y. Zhao, S. K. Cho, Proceedings of 2005 IEEE International Conference on Robotics and Biomimetics (IEEE ROBIO 2005), Hong Kong SAR and Macau SAR, 2005, 269–273.
18 J. L. Jackel, J. J. Johnson and W. J. Tomlinson, Bistable optical switching using electrochemically generated bubbles, *Opt. Lett.*, 1990, **15**, 1470–1472.

19 D. A. Ateya, A. A. Shah and S. Z. Hua, An electrolytically actuated micropump, *Rev. Sci. Instrum.*, 2004, **75**, 915–920.
20 D. A. Ateya, A. A. Shah and S. Z. Hua, Impedance-based response of an electrolytic gas bubble to pressure in microfluidic channels, *Sens. Actuators, A*, 2005, **122**, 235–241.
21 H. Suzuki and R. Yoneyama, Integrated microfluidic system with electrochemically actuated on-chip pumps and valves, *Sens. Actuators, B*, 2003, **96**, 38–45.
22 S. Z. Hua, F. Sachs, D. X. Yang and H. D. Chopra, Microfluidic actuation using electrochemically generated bubbles, *Anal. Chem.*, 2002, **74**, 6392–6396.
23 X. Geng, H. Yuan, H. N. Oguz and A. Prosperetti, Bubble-based micropump for electrically conducting liquids, *J. Micromech. Microeng.*, 2001, **11**, 270–276.
24 T. G. Leighton, *The Acoustic Bubble*, Academic Press, San Diego, CA, 1997.
25 P. Marmottant and S. Hilgenfeldt, Controlled vesicle deformation and lysis by single oscillating bubbles, *Nature*, 2003, **423**, 153–156.
26 P. Marmottant and S. Hilgenfeldt, A bubble-driven microfluidic transport element for bioengineering, *Proc. Natl. Acad. Sci. U. S. A.*, 2004, **101**, 9523–9527.
27 T. Cubaud, M. Tatineni, X. L. Zhong and C. M. Ho, Bubble dispenser in microfluidic devices, *Phys. Rev. E: Stat. Phys., Plasmas, Fluids, Relat. Interdiscip. Top.*, 2005, **72**, 037302.
28 J. M. Gordillo, Z. Cheng, A. M. Ganan-Calvo, M. Ma'rquez and D. A. Weitzb, A new device for the generation of microbubbles, *Phys. Fluids*, 2004, **16**, 2828–2834.
29 P. Garstecki, I. Gitlin, W. DiLuzio, G. M. Whitesides, E. Kumacheva and H. A. Stone, Formation of monodisperse bubbles in a microfluidic flow-focusing device, *Appl. Phys. Lett.*, 2004, **85**, 2649–2651.
30 J. H. Xu, S. W. Li, Y. J. Wang and G. S. Luo, Controllable gas-liquid phase flow patterns and monodisperse microbubbles in a microfluidic T-junction device, *Appl. Phys. Lett.*, 2006, **88**, Art. No. 133506.
31 P. Garstecki, M. J. Fuerstman, H. A. Stone and G. M. Whitesides, Formation of droplets and bubbles in a microfluidic T-junction – scaling and mechanism of break-up, *Lab Chip*, 2006, **6**, 437–446.
32 P. Garstecki, M. J. Fuerstman and G. M. Whitesides, Oscillations with uniquely long periods in a microfluidic bubble generator, *Nat. Phys.*, 2005, **1**, 168–171.
33 D. D. S. Meng, J. Kim and C.-J. Kim, A degassing plate with hydrophobic bubble capture and distributed venting for microfluidic devices, *J. Micromech. Microeng.*, 2006, **16**, 419–424.
34 T. Ito, T. Torii and T. Higuchi, IEEE 16th International Conference on Microlectromechanical Systems, Kyoto, Japan, 2003, 335–338.
35 Y. Zhao and S. K. Cho, Proceedings of 2005 International Conference on Microchannels and Minichannels, Toronto, Canada, 2005, ICMM2005-75154.
36 M. G. Lippmann, Relations entre les phénomènes electriques et capillaires, *Ann. Chim. Phys.*, 1875, **5**, 494–549.
37 B. Berge, Electrocapillarity and wetting of insulator films by water, *C. R. Acad. Sci., Ser. II: Mec., Phys., Chim., Sci. Terre Univers*, 1993, **317**, 157–163.
38 F. Mugele and J.-C. Baret, Electrowetting: From basics to applications, *J. Phys.: Condens. Matter*, 2005, **17**, R705–R774.
39 K.-L. Wang and T. B. Jones, Electrowetting dynamics of microfluidic actuation, *Langmuir*, 2005, **21**, 4211–4217.
40 J. Zeng and T. Korsmeyer, Principles of droplet electrohydrodynamics for lab-on-a-chip, *Lab Chip*, 2004, **4**, 265–277.
41 B. S. Gallardo, V. K. Gupta, F. D. Eagerton, L. I. Jong, V. S. Craig, R. R. Shah and N. L. Abbott, Electrochemical principles for active control of liquids on submillimetre scales, *Science*, 1999, **283**, 57–60.
42 O. D. Velev, B. G. Prevo and K. H. Bhatt, On-chip manipulation of free droplets, *Nature*, 2003, **426**, 515–516.
43 P. R. C. Gascoyne, J. V. Vykoukal, J. A. Schwartz, T. J. Anderson, D. M. Vykoukal, K. W. Current, C. McConaghy, F. F. Becker and C. Andrews, Dielectrophoresis-based programmable fluidic processors, *Lab Chip*, 2004, 4.
44 D. E. Kataoka and S. M. Troian, Patterning liquid fow on themicroscopic scale, *Nature*, 1999, **402**, 794–797.
45 T. A. Sammarco and M. A. Burns, Thermocapillary pumping of discrete drops in microfabricated analysis devices, *AIChE J.*, 1999, **45**, 350–366.
46 K. Ichimura, S.-K. Oh and M. Nakagawa, Light-driven motion of liquids on a photoresponsive surface, *Science*, 2000, **288**, 1624–1626.
47 H. Moon, S. K. Cho, R. L. Garrel and C.-J. Kim, Low voltage electrowetting-on-dielectric, *J. Appl. Phys.*, 2002, **92**, 4080–4087.
48 S. K. Cho, H. Moon and C.-J. Kim, Creating, transporting, cutting and merging of liquid droplets by electrowetting-based actuation for digital microfluidic circuits, *J. Microelectromech. Syst.*, 2003, **12**, 70–80.
49 J. Lee, H. Moon, F. Fowler and C.-J. Kim, Electrowetting and electrowetting-on-dielectric for microscale liquid handling, *Sens. Actuators, A*, 2002, **95**, 259–268.
50 M. G. Pollack, R. B. Fair and A. D. Shenderov, Electrowetting-based actuation of liquid droplets for microfluidic applications, *Appl. Phys. Lett.*, 2000, **77**, 1725–1726.
51 M. G. Pollack, R. B. Fair and A. D. Shenderov, Electrowetting-based actuation of droplets for integrated microfluidics, *Lab Chip*, 2002, **2**, 96–101.
52 V. Srinivasan, V. K. Pamula and R. B. Fair, An integrated digital microfluidic lab-on-a-chip for clinical diagnostics on human physiological fluids, *Lab Chip*, 2004, **4**, 310–315.
53 A. R. Wheeler, H. Moon, C. A. Bird, R. R. O. Loo, C.-J. Kim, J. A. Loo and R. L. Garrell, Digital microfluidics with in-line sample purification for proteomics analyses with maldi-ms, *Anal. Chem.*, 2005, **77**, 534.
54 A. R. Wheeler, H. Moon, C.-J. Kim, J. A. Loo and R. L. Garell, Electrowetting-based microfluidics for analysis of peptides and proteins by matrix-assisted laser desorption/ionization mass spectrometry, *Anal. Chem.*, 2004, **76**, 4833.
55 Y. Zhao and S. K. Cho, Microparticle sampling by electrowetting-actuated droplet sweeping, *Lab Chip*, 2006, **6**, 137–144.
56 P. Collet, J. De Coninck, F. Dunlop and A. Regnard, Dynamics of the contact line: Contact angle hysteresis, *Phys. Rev. Lett.*, 1997, **79**, 3704–3707.
57 E. L. Decker and S. Garoff, Contact line structure and dynamics on surfaces with contact angle hysteresis, *Langmuir*, 1997, **13**, 6321–6332.
58 C. W. Extrand, A thermodynamic model for contact angle hysteresis, *J. Colloid Interface Sci.*, 1998, **207**, 11–19.

